Characterization of the conductivity of metal-oxide interface of zirconium based fuel cladding at low and high burnups

Hawes, Jonathan; Baris, Adrienn; Chiu, Yu-Lung; Abolhassani, Sousan

DOI:
10.1016/j.jnucmat.2020.152133

Document Version
Peer reviewed version

Citation for published version (Harvard):
Hawes, J, Baris, A, Chiu, Y-L & Abolhassani, S 2020, 'Characterization of the conductivity of metal-oxide interface of zirconium based fuel cladding at low and high burnups', *Journal of Nuclear Materials*, vol. 534, 152133, pp. 1-12. https://doi.org/10.1016/j.jnucmat.2020.152133

Journal Pre-proof

Characterization of the conductivity of metal-oxide interface of zirconium based fuel cladding at low and high burnups

Jonathan Hawes, Adrienn Baris, Yu-Lung Chiu, Sousan Abolhassani

PII: S0022-3115(19)31278-4

DOI: https://doi.org/10.1016/j.jnucmat.2020.152133

Reference: NUMA 152133

To appear in: *Journal of Nuclear Materials*

Received Date: 3 October 2019

Revised Date: 17 February 2020

Accepted Date: 23 March 2020

Please cite this article as: J. Hawes, A. Baris, Y.-L. Chiu, S. Abolhassani, Characterization of the conductivity of metal-oxide interface of zirconium based fuel cladding at low and high burnups, *Journal of Nuclear Materials* (2020), doi: https://doi.org/10.1016/j.jnucmat.2020.152133.

Author statement

Jonathan Hawes: Methodology, Validation, Formal analysis, Investigation, Writing - Original Draft, Writing - Review & Editing, Visualization

Adrienn Baris: Investigation, Writing - Original Draft, Writing - Review & Editing

Yu-Lung Chiu: Writing - Review & Editing, Supervision, Project administration

Sousan Abolhassani: Conceptualization, Methodology, Validation, Resources, Writing - Original Draft, Writing - Review & Editing, Visualization, Supervision, Project administration

Characterization of the conductivity of metal-oxide interface of zirconium based fuel cladding at low and high burnups

Jonathan Hawes[1] *, Adrienn Baris[1], Yu-Lung Chiu[2] and Sousan Abolhassani[1]
[1]*Laboratory for Nuclear Materials, Nuclear Energy and Safety, Paul Scherrer Institut, 5232 Villigen PSI, Switzerland*.
[2]School of Metallurgy and Materials, University of Birmingham, B15 2TT Birmingham, United Kingdom
***Corresponding author: jonathan.hawes@psi.ch**

Abstract

In this study the conductivity/resistivity of oxide formed on Zircaloy-2 nuclear fuel cladding is measured. The same cladding grade (LK3/L) is used to compare the oxide formed after short and long residence times, respectively 3 and 9 cycles, in a Boiling Water Reactor (BWR). The oxide in the vicinity of the metal-oxide interface is studied. The measurements were carried out using a novel technique developed at PSI, using micromanipulators (micromanipulator) inside a FIB/SEM to probe different thicknesses of oxide and hence directly measure the resistance and calculate the resistivity of that thickness of oxide. The results from the 3 and 9 cycle oxides are compared. It is demonstrated that the resistivity of the oxide in the vicinity of the interface of the 9-cycle cladding increases with distance from the interface, much faster than that of 3-cycle cladding to a maximum level. The study is correlated to previous work, performed at PSI, characterizing these 2 materials by EPMA and other techniques.

1 Introduction

Zirconium alloys have been used since the early 1950's as nuclear materials [1] and in the 1960's became the most commonly used material for fuel cladding in light water and heavy water reactors [1]. Hydrogen uptake and subsequent hydride formation during component lifetime has been identified as one of the critical life limiting degradation behaviours for these components [2]–[5]. It has been demonstrated by recent studies that hydrogen uptake is not constant throughout component lifetime and it can increase or decrease with residence time [4], [6]. To explain the mechanism of hydrogen uptake and its variation from one alloy to another, (or for the same alloy at different stages of oxidation and irradiation), the oxide electronic resistivity is considered. It is claimed that this parameter plays a significant role in the corrosion kinetics and hydrogen pickup. In other words, one of the hypothesis is that increasing oxide resistivity would decrease the mobility of electrons from the metal-oxide interface, where the oxidation reaction takes place, out to the oxide-water interface. This in turn would increase the electrical potential across the oxide and hence the driving force for the ingress of positive H^+ ions [2], [7], [8].

This implies that, in the process of oxidation and hydrogen uptake, the metal-oxide interface and oxide-water interface and the pre-existing oxide layer separating the two interfaces function similar to an electrochemical cell [9]. Either negatively charged electrons must migrate outwards, through the oxide to reduce positive H^+ ions at the oxide-water interface; or H^+ ions must ingress through the oxide, to capture the electrons. The latter is unfavourable, as the hydrogen being very close to the metallic site, can cause a rapid ingress of hydrogen into the underlying metal and increase the hydrogen uptake. Above a certain level of concentration, at the service temperature hydrogen will precipitate in the form of hydrides and can lead to cladding embrittlement and a loss of mechanical properties [2], [4].

In order to verify the above-mentioned hypothesis, it is useful to measure the resistivity of oxide in the vicinity of metal-oxide interface and at an increasing distance into the oxide, and compare two materials with two different hydrogen pick-up fractions (HPUF).

Previous attempts have been made to quantify the resistivity of the oxide by Electrochemical Impedance Spectroscopy (EIS) [8], [10]–[16]. There are some limitations to this technique, firstly since in most cases, the experiments are performed in autoclave conditions there is an absence of irradiation and related in reactor phenomena (e.g. changes of microstructure, chemical composition and irradiation induced defects and furthermore, gradual changes of water chemistry). Secondly, since the samples are immersed in electrolyte, it is not possible to have a direct measurement of intrinsic oxide resistivity but instead a bulk average is calculated across the whole sample; and the exact thickness of the oxide probed is unknown. This technique has been successfully paired with weight gain measurements[8], [11], [12], [14], which can be correlated to oxide thickness but once again the electrolyte is expected to penetrate into the oxide through open pores and cracks, and hence modify its properties. Furthermore, the exact penetration distance measured in the oxide is unknown.

The objective of the current work is to determine the inherent (in the absence of external parameters) oxide conductivity near the metal oxide interface of a Zircaloy-2 (LK3/L grade) and to compare the variations after 3 and 9 cycles of irradiation in a Swiss boiling water reactor (Kernkraftwerk Leibstadt, KKL). The measurements were performed, by means of a novel technique developed at the laboratory, Paul Scherrer Institut (PSI). Using micromanipulators (micromanipulator) in a scanning electron microscope (SEM), the resistivity of a certain thickness of oxide at a certain point could be directly measured. Although this paper will cover to some extent the experimental method, further detail for the hydrogen measurements and for the conductivity technique can be found in refs [6] and [17], [18]. The results will then be compared with the hydrogen uptake for both materials, previously measured in ref. [6].

The choice of material in this study is based on the analysis of a high burnup LK3/L cladding, which after 9-cycles in reactor had still a surprisingly satisfactory oxidation behaviour; however, it showed an increase in hydrogen pickup fraction. It should be kept in mind that this material is not designed to stay for such long residence times in reactor, and the 9-cycle cladding was produced for research activities only. The hydrogen pickup fraction of the cladding after 9 cycles had reached 30% compared to the 3-cycle cladding which was 17% [6]. This finding forms the basis for the motivation for the extensive characterisation and comparison of its high and low burnup samples [6], [19]–[23]. The advantage of this technique is the capability to measure the oxide conductivity at site specific regions of the material and provide the intrinsic properties of the region analysed.

2 Materials and method

2.1 Materials analysed

As explained above, in order to compare the state of a highly irradiated material with another of low irradiation, a 9 and a 3 annual cycle sample were chosen. Particularly of interest is the last oxide formed at these two different stages of life, i.e. the very inner oxide at metal-oxide interface. The material is Zircaloy-2 LK3/L grade, the composition is shown in Table 1.

Table 1. The chemical composition for both a standard Zircaloy-2 and the LK3/L grade. The designation /L indicates the presence of an inner liner on the cladding [6]

Composition (wt%)	Sn	Fe	Cr	Ni	Fe+Cr+Ni	O ppm	Si ppm
Standard Zircaloy-2 ASTM (B353)	1.2-1.7	0.07-0.2	0.05-0.15	0.03-0.08	0.18-0.38	1000-1400	Maximum 120
LK3/L	1.34	0.18	0.11	0.05	0.34	1320	70

The investigated segments are from similar elevation and position in the rod assembly to allow direct comparison. The 9-cycle segment has a local burnup of 89 MWd/kgU, and the 3-cycle a local burnup of 41 MWd/kgU. More details on the rod burn up, segment elevation, mean oxide thickness and total hydrogen content are shown in Table 2. Further description of samples and of heat treatment can be found in [6].

Table 2. Measured data for 3 and 9-cycle Lk3/L claddings [6].

Sample	Rod average burn-up (MWd/kgU)	Segment elevation (mm)	Mean oxide thickness (μm)	Total Hydrogen content (ppm)
3-cycle LK3/L	36	2011	4.4 ($\pm$0.7)	44
9-cycle LK3/L	78.7	2039	46 ($\pm$2.5)	595

2.2 Experimental technique and instrumentation

A focused ion beam (FIB) has been used to micro-machine the samples. The instrument was a Zeiss NVision40 dual-beam SEM-FIB system. Subsequent to the micro-fabrication of segments, micromanipulators from Imina Technologies dedicated for such measurements were used to measure the conductivity. The overall experiment has 4 steps as follows: a) micro-machining of the wedges at metal-oxide interface, b) deposition of Pt electrodes by electron beam, c) measurement of conductivity by micromanipulator and d) cutting under the electrodes to measure the exact thickness of underlying oxide.

The details of the experiment are further outlined below: first, the outer oxide is removed using a high current in the FIB. Then the current is reduced to create a wedge shape from the inner oxide at a small angle of 2° w.r.t. the metal-oxide interface, leading to a wedge with varying oxide thickness. Platinum

electrodes can then be deposited over this wedge. In this manner, beneath each electrode a band of oxide with increasing thickness is present, before reaching the underlying Zr metal (Figure 1.a). Furthermore, there was also one electrode deposited where no oxide was left i.e. on the polished metal. This was used as a reference of the whole circuit without containing any thickness of oxide for each wedge. To complete the circuit an electrode is also prepared on polished Zr metal at a given distance (usually in the region of 100-300μm) away from the wedge, and at an orientation perpendicular to the surface of the wedges. Figure 1.a depicts well this configuration. To reduce the different errors, the area of Pt electrode deposited for every oxide thickness was kept constant at a size of 4 μm x 8 μm. The thickness of the Pt deposition was also kept in the range of a few hundred nm. Using micromanipulators inside the SEM both the metal electrode and the wedge oxide electrode can be contacted simultaneously to form a circuit. Included in the circuit is an ammeter capable of reading very low currents, hence high resistances (in this case a Keithly 6487 pico-ammeter). When a voltage is then applied, the circuit will consist of the metal region, the thin Pt depositions and a certain thickness of oxide. This oxide thickness varies, depending on which electrode is contacted with the micromanipulator. During this experiment, a DC voltage of 0.1V was applied. Although higher voltages did prove to give less error for larger oxide thicknesses (or much higher resistances), this low voltage was chosen a- to be sure the voltage limit (the so-called breaking voltage) was not reached and b- to be consistent with previous work [17], [18]. A schematic diagram of the circuit set-up when contacted with micromanipulator is shown in Figure 1.b. A more detailed description of the experimental technique and set-up is provided in [17], [18]**.** An example of the position of electrodes on the oxide is shown in Figure 2. The micromanipulator tips can be observed in operation inside the SEM in Figure 3.a and the contacting of the electrodes is shown in Figure 3.b.

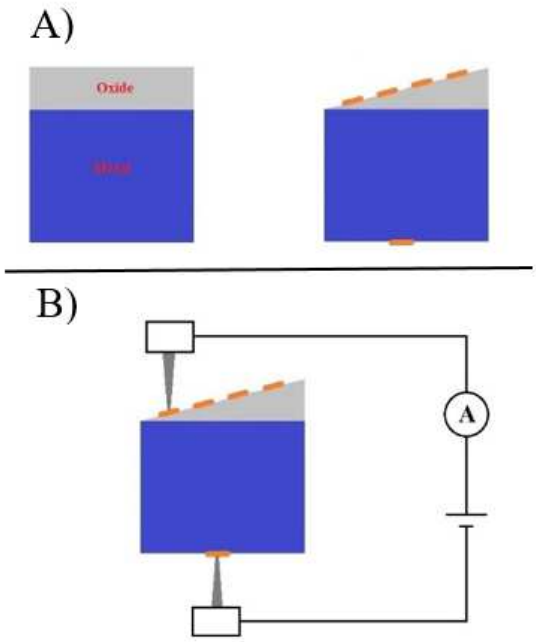

Figure 1. Schematic diagram of the set up used to measure conductivity A) shows the oxide wedge with the deposited electrodes (exaggerated) and one electrode deposited a distance away on the metal B) shows the micromanipulators contacting the first oxide electrode and the metal electrode deposited in a different place to form a circuit. [17], [18]

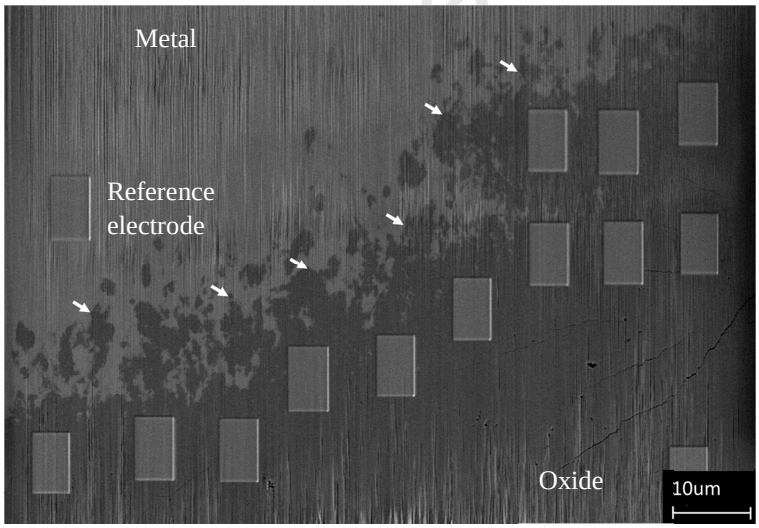

Figure 2. SEM image of electrodes deposited onto the oxide wedge for 3-cycle sample. The metal (bright contrast) and oxide (dark contrast) regions of the wedge are indicated. The electrodes can be clearly seen on the oxide and an additional electrode was deposited on the bare metal region to allow a reference value to be measured i.e. the resistance of the circuit without containing any oxide. Arrows point to the approximate region of metal-interface, due to the angle of polish.

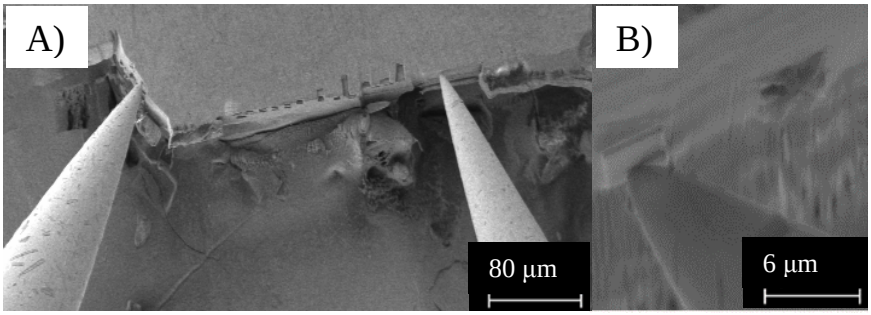

Figure 3. SEM image of the 9-cycle sample, a) Micromanipulator tips and setup in the SEM ready to measure the electrodes, distance between the two electrodes is approximately 200 µm. b) Illustrating the contact between micromanipulator tip and electrode

2.3 Determination of the exact oxide thickness under each electrode

In the 9 cycle material the oxide can also be identified by the many cracks. After the measurement each electrode was cut to reveal the exact oxide thickness beneath it, this was done using the SEM FIB and examples are shown in Figure 4. The majority of electrodes were cut in two different locations in an attempt to find the minimum oxide thickness, due to the undulating nature of the oxide. The oxide could be viewed when the contrast is enhanced as the darker material. In the 9 cycle material the oxide can also be identified by the many cracks. Effort was made to determine this minimum oxide thickness but the possibility of the existence of a thinner section of oxide, due to undulation, under the electrode must be kept in mind. In the oxide layers with a thinner average thickness, larger percentage change would exist if an unknown undulation was present. For some electrodes, covering very large thicknesses of oxide, only space for one cut was available; in these instances, attempt was made to watch the cutting procedure for any large irregularities in oxide thickness.

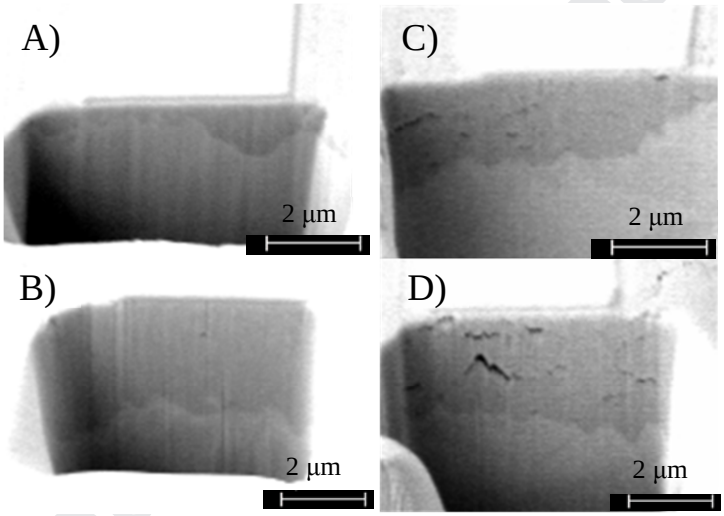

Figure 4. SEM images of the oxide found beneath electrodes. Figures a) and b) the oxide of the 3-cycle material; Figures c) and d) the 9-cycle material. The contrast is greatly enhanced to allow identification of the darker contrast oxide and hence measure the thickness under each electrode. In the 9-cycle material, the oxide can be identified by the many cracks.

2.4 Calculation of results and assumptions

The resistivity values were calculated from the measured resistance for each electrode using the formula,

$$\rho = \frac{RA}{l}, \qquad \textit{(Equation 1)}$$

Where ρ is resististivity, R is resistance, A is area, and l is length.
To calculate the resistivity in this manner some assumptions were made. As can be seen in Figure 2, besides the electrodes on the oxide wedge there were also reference electrodes in contact with the metal in the wedge to measure the resistance of the set up using the conductivity of metal Zr as our base point or reference point. The measured resistance, using these reference electrodes of the Zr metal with such setup ranged between 30-150 ohms, and hence was considered negligible compared to the measured resistance values from the oxide electrodes which ranged between $10^4 - 10^9$ ohms. Thus one assumption was that the setup together with the conducting metal has a very low resistance.

The creation of a contact between a semi-conductor and a metal in the semi-conducting field is the

precursor for the fabrication of low voltage drop diodes and it is quite well known. In the case of the present study, the aim being to probe the property of the "semi-conductor", i.e. the substoichiometric oxide, which is equivalent of the n-type semi-conductor of the so-called Schottky barrier diodes, this aspect of the setup is only needed for the facility of measurements. However, in order to verify, if the deposition of Pt plays a role on the modifications of the measurements, the conclusion from bulk studies performed previously [24] is reported here. This effect has been previously studied using various electrode metal materials on zirconium oxides [24], it was concluded that "No visible effects of electrode materials on the specimen current of zircaloy oxides are found [24]." With these assumptions in mind it is clear that the importance of this work lies within the comparison between the two materials and hence any effects which may arise would be systematic and the comparison still valid. In other words, it is assumed that if any effect would exist, as it is more or less similar for all electrodes, the comparative analysis will hold.

Therefore, it is concluded that the assumption that the object length contributing to the high resistivity being probed is solely the thickness of oxide beneath the electrode, is valid. For these calculations, always the minimum oxide thickness found under each electrode, is used as length. Although every electrode was built to have the same dimensions of 4 μm x 8 μm, the thickness of underlying oxide was not constant, and therefore, not a single number could be used to represent this thickness. As it can be clearly seen from Figure 4 the minimum thickness of oxide is not constant below each electrode over the whole area of Pt, since the oxide interface is undulated. This undulation has been reported many times and is a well known phenomenon [25]–[27] with the area of an average protrusion calculated to be approximately 0.9 μm x 0.9 μm. Hence, the path of the current beneath each of the electrodes cannot be totally known. For this reason, a minimum value of resistivity was calculated using the protrusion area and a maximum calculated using the total electrode area. An average of these two values has been adopted for this study (Table 3 and Table 4).

3 Results

The full oxide thickness formed on the examined cladding, after 3 cycles and 9 cycles in reactor, is 4.4 μm and 46 μm respectively. However, the interest of the research focuses on the last oxide formed on the cladding. This layer in the case of Zr and its alloys is always the last layer in contact with the metal-oxide interface. For this reason the property of the oxide in the vicinity of the interface is of interest for the understanding of the mechanisms involved in oxidation and hydrogen uptake. Since the aim of the current study was to measure the resistivity of the oxide that has formed most recently, only this region from both claddings has been probed. This allows a direct comparison of the oxide formed at low and high burnups.

Tables containing the resistance measurements for the various electrodes and their respective minimum oxide thicknesses for both materials and all campaigns can be found in appendix A. From those results, the resistivities could be calculated as described in section 2.4. In each table, as well as the minimum thickness measured under each electrode and the measured resistance of that electrode, there is the lower and higher calculated resistivity values (calculated from a minimum or maximum area). Furthermore, a resistivity value taken from the average of these possible minimum and maximum is provided. Figure 5a, b and c contain the oxide resistivity results from both the 3 and 9-cycle samples displayed as a function of oxide thickness, on different scales to help better visualisation. The 'average resistivity' values are displayed in these graphs. The three sets of results come from three separate campaigns, with new cuts and new electrodes deposited on a fresh region of

the material, followed by a micromanipulator measurement and subsequent cutting of the new electrodes, for 3 and 9-cycle materials individually. Please note that while it appears that some resistivity values are close to zero for some oxide electrodes; this is an effect of the units. And it must be kept in mind that even the lowest resistivity values for oxide regions, which are in the range of 10^-2 $\Omega.m$ are still 5 orders of magnitude higher than that of the reference electrodes. Bearing in mind that reference electrodes are the zirconium metal with known resistivity. The resistivity of zirconium metal is in the range of 10^-6. This comparison can be clearly viewed in Figure 5d.

A)

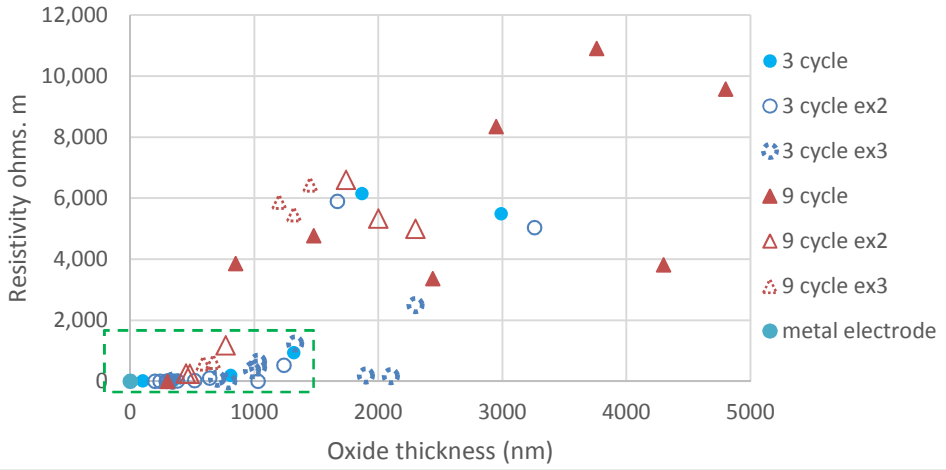
Resistivity (Av) vs Thickness
Resistivity ohms. m
12,000
10,000
8,000
6,000
4,000
2,000
0
0
1000
2000
3000
4000
5000
Oxide thickness (nm)
3 cycle
3 cycle ex2
3 cycle ex3
9 cycle
9 cycle ex2
9 cycle ex3
metal electrode

B)

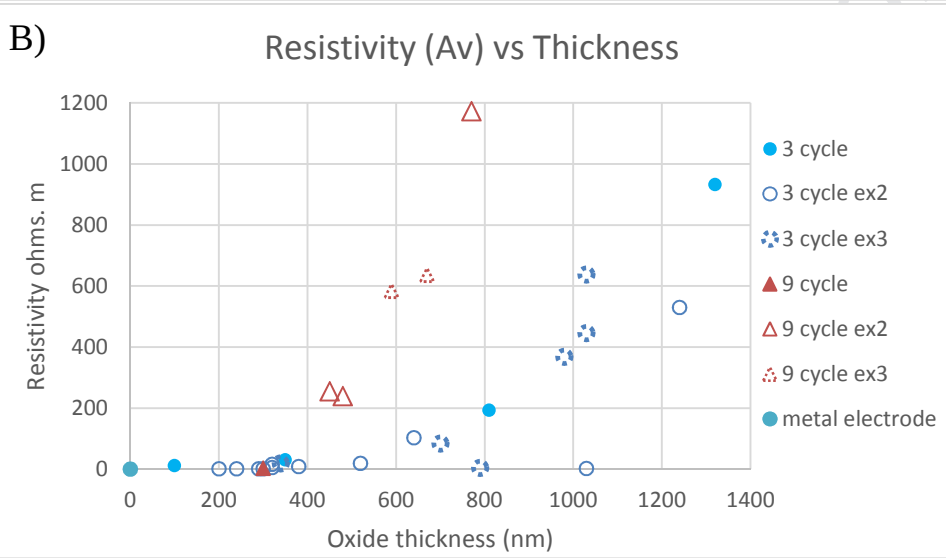
Resistivity (Av) vs Thickness
Resistivity ohms. m
1200
1000
800
600
400
200
0
0
200
400
600
800
1000
1200
1400
Oxide thickness (nm)
3 cycle
3 cycle ex2
3 cycle ex3
9 cycle
9 cycle ex2
9 cycle ex3
metal electrode

C)

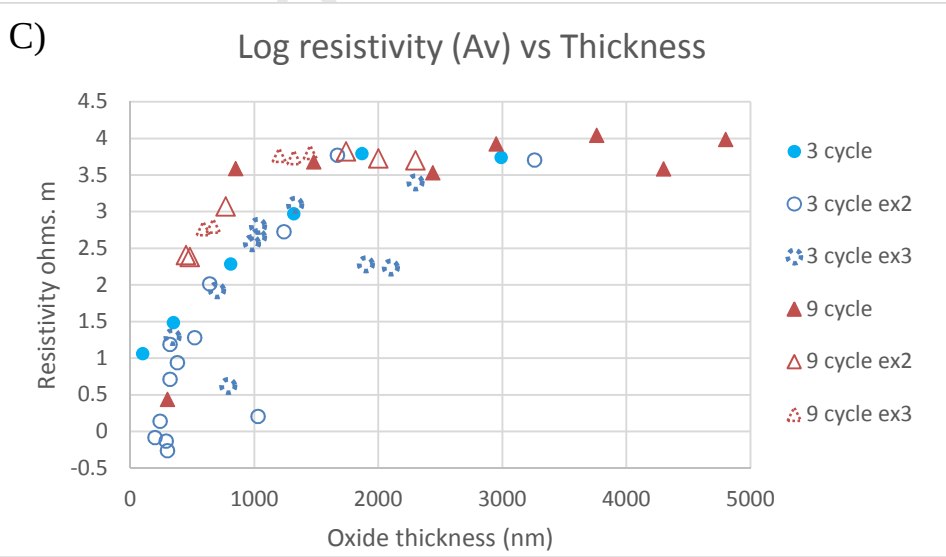
Log resistivity (Av) vs Thickness
Resistivity ohms. m
4.5
4
3.5
3
2.5
2
1.5
1
0.5
0
-0.5
0
1000
2000
3000
4000
5000
Oxide thickness (nm)
3 cycle
3 cycle ex2
3 cycle ex3
9 cycle
9 cycle ex2
9 cycle ex3

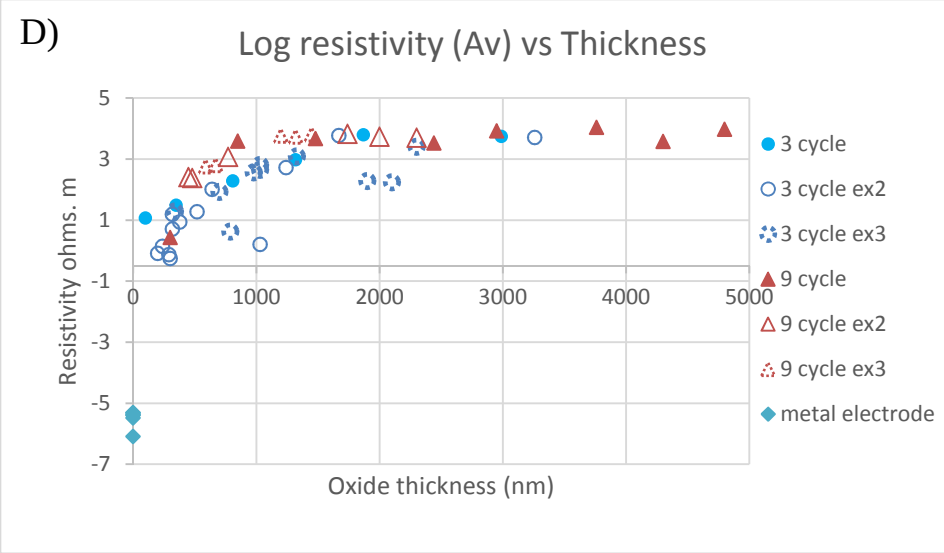

Figure 5. a) Graph showing the resistivity vs oxide thickness for 3 cycle oxide (shown as blue circles) and 9 cycle oxide (shown as red triangles) each point is a different electrode. b) Is a selection of points from graph (a) expanded to show the trend at thin oxide thicknesses, the region to be expanded is shown in (a) by a green dashed box. c) Graph showing the log of resistivity vs oxide thickness for 3 cycle oxide (shown as blue circles) and 9 cycle oxide (shown as red triangles). d) Same as graph (c) but also including the resistivity values of the Zr reference electrodes for reference. For each graph a difference in marker outline is made between the results from campaign 1, 2 and 3.

3.1 Examination of resistivity of control samples

Before interpreting further the outcome of the studies and the difference between the two sets of measurements, attempt is made here to confirm the reliability of the measurements and the setup. For that, the resistance of different control samples is measured in the SEM/FIB using micromanipulator, in very similar configurations. The chosen materials were I. a $10M\Omega$ *resistor, II. ZrO powder and III. p-doped Silicon with a known resistivity of 0.01-0.2*$\Omega.m$*. Furthermore, it is considered that many Zr to Zr reference electrodes measured in each trial of the experiment, are absolutely best types of "internal" references. The resistor and doped silicon were chosen to be measured, with the set up, to calibrate and confirm the values produced by this technique. Micrographs indicating the samples during measurements for these references can be seen in Figure 6 and*

Figure 7 respectively. Measurement of the resistor consistently returned values of $10M\Omega$ *within a 5% tolerance. The doped silicon had Pt electrodes deposited (of dimensions 4 μm x 8 μm) and was measured at applied voltages between 0.1V and 1V. Using the area of electrodes and being tested as shown in*

Figure 7 a mean value of $0.043 \pm 0.010\ \Omega.m$ was measured, which is in good agreement with the known resistivity. For ZrO powders the aim of the test was to confirm the linear response of resistance vs distance between the micromanipulator tips, as well as the effect of varying the applied voltage. Furthermore, it was planned to study a sample without any FIB alteration, so that the material does not contain any Ga contamination. Different powder particles were contacted with the micromanipulators across different distances and the resistance was measured. One example of the measurement configuration and the ZrO particles can be seen in Figure 8. The results are plotted in Figure 9 and confirm a linear response furthering the reliability of the set up (the values for distance may vary due to the no uniform shape of the particle). This gave a value of resistivity of 6.6 x 10^-6$\Omega.m$ $\pm$2.5 x 10^-6$\Omega.m$ with the assumption that the contact tips were1.5 μmx1.5 μm squares. At certain positions, the applied voltage was varied between 0.05V and 1V. The returned resistance remained constant with a maximum deviation of +/- 10%. This confirms an ohmic response as expected; this may facilitate in the future the increase of the applied voltage for highly resistive materials in order to reduce the effect of 'noise' within the system. For example a rough limit of the measureable resistance attainable is, for 0.1V in the magnitude of $10^9\ \Omega$, for 1V in the magnitude of $10^{10}\ \Omega$ and for 10V in the magnitude of $10^{11}\ \Omega$.

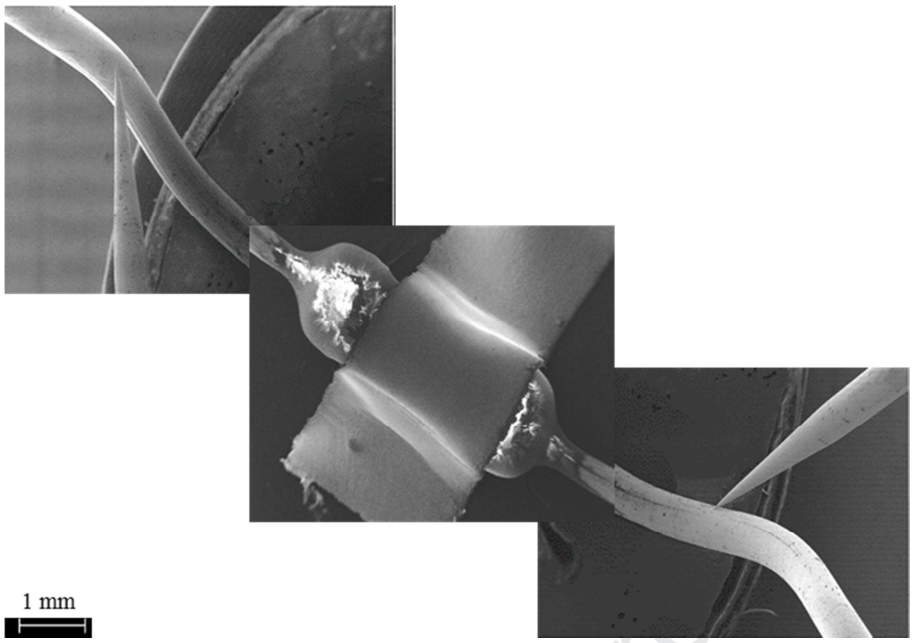

Figure 6. The measurement of a 10MΩ resistor with the two tips contacting the wire on either side of the resistor. The two sides are shown here separately, since the object is too large to be captured in one SEM image. Here there is direct tip metal contact without an electrode. Only resistance was being measured not resistivity.

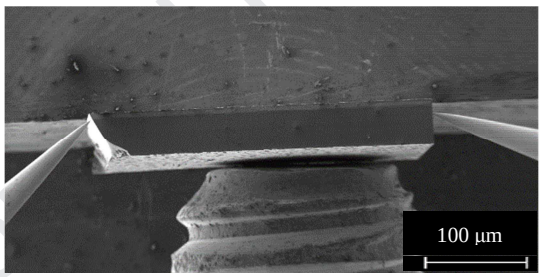

Figure 7. The measurement of p-doped silicon wafer, here tips can be seen in position with silicon of length of 3.4 mm

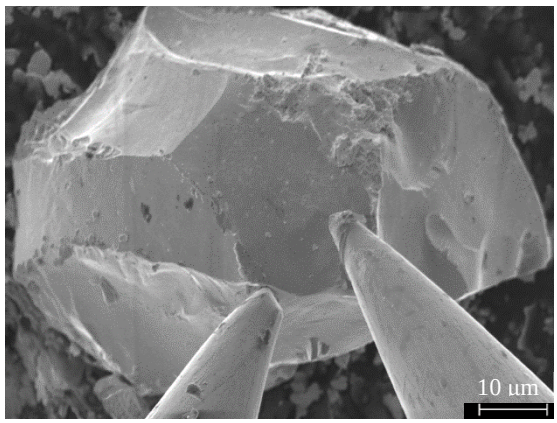

Figure 8. Micromanipulator tips contacting a particle of ZrO with a small separation distance

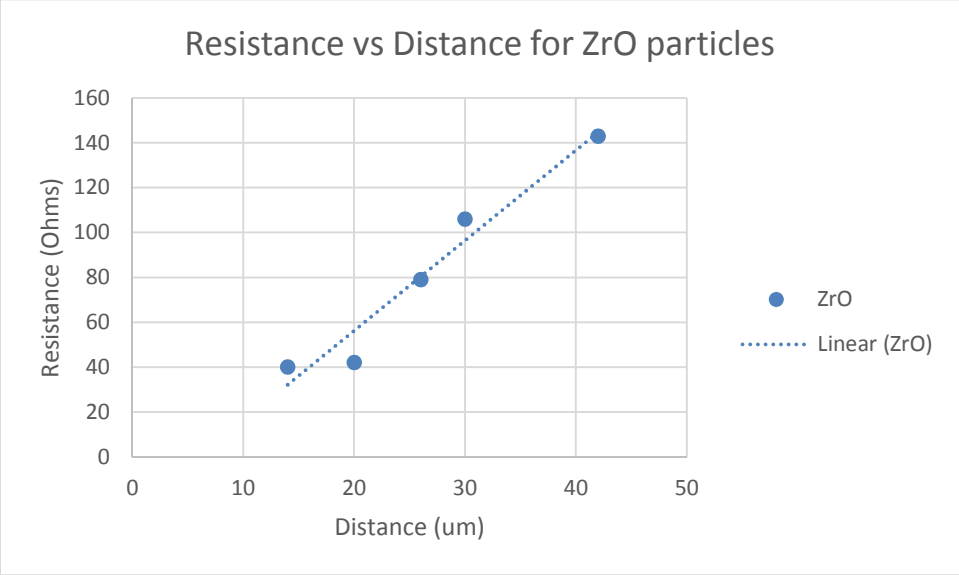

Figure 9. Graph of the resistance measured with a 0.1V applied across varying distances. Results show a linear trend so that resistance increases with distance probed, and resistivity remains constant as the particle has a uniform composition.

4 Discussion

4.1 The scope of technique

As previously mentioned this is a novel technique developed at PSI with the aim to achieve two previously unachieved goals. Firstly to examine the conductivity of irradiated materials, in particular the oxide formed in reactor on zirconium based alloys. Secondly to obtain direct resistivity measurements from regions of pre-existing oxide i.e. to see the resistivity of specific regions of oxide rather than the resistivity over a whole oxide film. This study shows that these goals have been well achieved.

The advantages of this method are as follows:

I. The technique so far has shown good repeatability within the scope of measurements, the deposition of Pt electrodes facilitates the use of micromanipulator and the confidence about the complete and repeatable contact between the micromanipulator and the sample. Performing the experiment within the SEM makes it possible to visualise the placement of micromanipulator and its contact with electrodes.
II. The small scale of this experiment allows the probing of exact locations within the oxide; this gives local resistances for known thicknesses of oxide.
III. The micromachining with FIB allows selecting the regions of interest with accuracy and creating electrodes at sensitive regions of the sample.
IV. This setup has shown the possibility of direct resistivity measurements for irradiated samples.
V. As it is possible to create very miniature cross sections, it is possible to demonstrate that at very small distance from the metal-oxide interface, different materials will not behave similarly.

In the following, the precautions to be taken to provide a satisfactory experiment are listed:

I. The sample preparation and the FIB polishing will influence the amount of damage induced by ions and the quality of surface. Which in turn could modify the properties of the oxide and its resistivity. Therefore, care should be taken to provide a surface that is as clean and intact from ion implantation and amorphization as possible.
II. With many cables and electronics of micromanipulator inside the SEM, care must be taken to install the micromanipulator in correct positions on its stage, with respect to the SEM gun and to consider that the displacement of micromanipulator should be within the range that is tolerated in the SEM.
III. The metal-oxide interface of different alloys and after different stages in the reactor, have very variable morphology. This would lead into a more or less undulated oxide at the interface. As an example, in the case of 3-cycle oxide a large variation of resistivity is observed for thinner oxides. This large variation can be directly correlated to the large undulation of the oxide at interface (as an example please refer to Figure 5, where a group of points between 200-300 nm show much lower resistivity and to Figure 2 which shows the very broad region where metal and oxide co-exist). The large undulations induce some uncertainty in the exact determination of the oxide thickness for thin oxides. Although the precaution should be taken to interpret the results, this is not a limitation of the technique but rather a specificity of the material examined in this study.
IV. The comparison of the resistivities measured by this technique with measurements performed by in situ EIS on unirradiated Zircaloy-4 and Zr 2.5%Nb [8] give results that are not comparable. The results of that study give oxide resistivity in the range of 2-10 $M\Omega.\,\mathrm{m}$ (for inactive materials) for oxide thicknesses in the range of 1-8 μm, that is to say 1000 times

higher compared with current results. From the Tables 3 and 4 it can be observed that the maximum resistivity values are higher than the average values; and it might be more adapted to take that number. However, as the environment in which the materials are immersed will be different in the two cases, the influence of environment should not be neglected. As an example, the resistivity of deionized water is known to be quite high (in the range of 1.80E+07) [28]. This could influence the outcome of measurements. Furthermore, the in situ EIS is a bulk technique and cannot be compared with the current method, which shows a local high spatial resolution evaluation of these properties. To make further comments similar materials should be measured with the two techniques. Otherwise, it will not be possible to judge if the intrinsic properties of the regions studied are different, or the methodologies are causing this difference. It must be reminded that the current study is on irradiated materials, whereas the EIS was on unirradiated.

V. These measurements are to examine the intrinsic properties of the material after different residence times, but it should be made clear that the oxide is expected to have differing resistivities in reactor (due to elevated temperatures, different pressures, different environment and irradiation conditions).

4.2 Discussion of results

The fact that the two materials show different results indicates that under identical measurement conditions, the comparison of the results is valid. As was mentioned before, one of the hypothesis regarding the mechanism of hydrogen uptake of a zirconium based fuel cladding is that the resistivity of the oxide has a direct relationship with the pickup fraction during oxidation. In other words, hydrogen pickup fraction would increase with increasing oxide resistivity. In the case of different cladding materials with different chemistry and heat treatment, prior to irradiation, this has been shown by in situ EIS [8]. The role of irradiation and residence time in-reactor, remained to be verified. For this, it was interesting to check if the same cladding grade, having evolved with residence time, would show a change of resistivity which could be correlated to its change of hydrogen pickup fraction. As such material was available in the laboratory, it was possible to verify this phenomenon.

Using the micromanipulator method, for the first time, the resistivity of oxide formed in-reactor on a Zircaloy-2 at low and extremely high burnups could be directly measured and compared. In Figure 5 the oxide resistivity is plotted against the distance from the metal/oxide interface for a Zircaloy-2 LK3/L after 3 and 9 cycles in reactor.

The observations from these results can be summarised as follows:

- Both oxides have a region with lower resistivity close to the metal/oxide interface.
- Within that region, the resistivity increases with distance, in the direction away from the interface, until plateauing with values in the range of 6-10 $K\Omega.\,\mathrm{m}$.
- The distance of these lower resistivity regions is not the same for both materials. Approximately this above-mentioned region extends up to a distance of 1500 nm in the 3-cycle material and 800 nm in the 9-cycle material.

"The following explanation is proposed for these observations. Many authors have suggested that the oxide in fact consists of two different regions, an outer heavily cracked porous layer and an inner dense impermeable layer [6], [21], [25], [29], [30]. It is claimed that coolant can penetrate into these

outer cracks and hence only the inner dense layer, predominantly acts as a barrier to the penetration of oxidizing species [6], [21], [25], [29], [30]. For this condition to satisfy, an oxygen vacancy gradient formed across this region, following a parabolic trend could be expected with the highest vacancy concentration being at the metal/oxide interface [31], [32]. It has been shown that sub-stoichiometric zirconium oxide has a higher conductivity than stoichiometric oxides [33]–[35]. It is shown that ZrO_{2-x} is acting as an n-type semiconductor, in this manner fully ionised vacancies will act as electron donors and hence more electrons as charge carriers will increase the electronic conductivity of the material [33]–[35]. It is stressed here that this conductivity is much lower than that of metal (metal being at least 5-6 orders of magnitude more conducting) (please refer to Figure 5-D). The same has been widely shown for Titanium oxide [36]–[38] which is known to share many similarities with zirconium oxide regarding some behaviours. As well as for other metal-oxide systems such as ZnO [39]. Thus, if there was in fact a diffusion governed dense inner oxide layer it could be expected that the conductivity of this region would also follow a parabolic curve with highest conductivity (hence lowest resistivity) closest to the metal/oxide interface, where the highest oxygen vacancy concentration exists. Once more, bearing in mind that the values of resistivity even if they are relatively low in these oxide regions, they are far higher than that of the underlying metal.

Although the cuts under each measurement cannot be individually chemically and structurally characterised, several different characterisation of the current samples, by different methods have been already performed in the laboratory. This provide complementary information needed to further interpret the current results.

A very thorough chemical analysis of the metal-oxide interface of 3-cycle and 9-cycle cladding have been performed in the laboratory [21] and the distribution of alloying elements on the two sides of the interface have been reported. Regarding the oxygen concentration, Figure 10 provides a clear comparison between the two materials, with particular interest in the region close to the metal/oxide interface, published in [21]. As can be seen in Figure 5c) for the 3-cycle material, we do detect a parabolic trend for the intrinsic resistivity of the material. In the case of the 9-cycle sample, the same is valid although extended to a shorter distance. This trend of increase of resistivity matches well, for both samples, with the oxygen profiles obtained from the EPMA measurements performed on the same samples, shown in
Figure 10. As it can be observed, the oxygen profile in the case of the 3-cycle cladding increases to the stoichiometric oxide at a longer distance, compared to the 9-cycle oxide. Here, this comparative behaviour is sought, rather than the exact quantitative values. It must be mentioned that these bulk overall results are not possible to obtain by other analytical methods.
In other words, the oxygen diffusion profile exists for both samples; but is extended to a shorter distance in the case of 9-cycle sample. Surprisingly, the distances are also very similar in the measurements by these two very different techniques, of two very different properties (i.e. the chemical composition and the resistivity).

The correlation between the sub-stoichiometric oxide regions and their resistivities together with the knowledge that oxides with higher oxygen vacancy concentration (sub-stoichiometry) show lower resistivity as seen in [33]–[35] leads to the suggestion that in this case it is oxygen vacancies that lead to the existence of a more conductive region, close to the interface, seen in both materials.

This observation suggests that i) both materials have an inner dense region governed by diffusion; ii) the size of this diffusion layer decreases with time in reactor. The positive finding of this study is that the diffusion layer is still present and relative large in the case of the 9-cycle material, which is beyond design. Furthermore, as observed by 3-D tomography, by Baris et al. [22], the volume fraction of cracks in the vicinity of the metal-oxide interface of the 9-cycle material is higher than the 3-cycle material (respectively 4.9% and 0.19%). However, the current measurements demonstrate that the

material still does show a more conducive region that will protect the underlying metal; Nevertheless, with a different kinetics being present between 3 and 9 cycles.

It must be stressed that the 9-cycle cladding is a material used as experimental sample for exploring the limits of performance of this cladding and its residence time is beyond design [40].

It has been demonstrated that most alloying elements dissolve from the secondary phase particles (SPP) and increase the matrix concentration of each element [19], [22]. It is clear that alloying elements could also have an impact on the conductivity; however, knowing that all alloying elements could play a role and their effect could also cumulate or counter balance each other [41] their impact with time will require a much more in depth analysis and is outside the scope of this study.

Further to the chemical analysis, the microstructure of the metal-oxide interface has been analysed in depth and it has been demonstrated that the 9-cycle oxide near the interface is much more porous, please refer to Figure 4. The role of porosity on the different properties of the oxide have been discussed by other authors and also in the laboratory [42], [19], [22],[23]. In a study performed previously, other researchers have shown that the porosity increases the resistivity of the oxide [42]. Therefore, it can be concluded that at least two factors are clearly at the origin of the differences of conductivity between the two materials. The stoichiometry of the oxide in the vicinity of the interface, with the 9-cycle oxide having a thinner sub-stoichiometric region, and the oxide porosity.

One more factor which has been topic of several studies in the field of oxidation of Zr based alloys is the ratio of tetragonal zirconia present in the oxide film and its impact on the oxidation. To correlate this crystallographic property to the conductivity, seems to be a big challenge, for that it is necessary to perform direct measurement at nanometric scale of the two properties (crystal structure of the oxide and its conductivity), and if possible simultaneously or in parallel. Such measurements will be very demanding. Therefore, attempt here has been made to conclude from the data available in the laboratory, and the literature data available on bulk tetragonal zirconia.

The crystal structure of the 9-cycle cladding has been object of a study in the laboratory [43] by synchrotron radiation. The major oxide phase observed has been reported to monoclinic ZrO_2 and a very small ratio of tetragonal has been revealed by Micro-XAS analysis. This small phase has been mainly observed in the vicinity of the interface, however, not on a uniform and homogeneous distribution all along the interface. The results obtained in the laboratory for 3-cycle cladding show similar behaviour but with a slightly higher volume fraction of tetragonal (the exact ratio of tetragonal to monoclinic is not calculated due to its small quantity). These observations lead to the conclusion that the two oxide layers (of 3 and 9 cycle) near the interface have mainly a monoclinic crystal structure, however a slightly higher proportion of tetragonal is present in the low burnup oxide. Therefore, as the measurements cover quite large areas and knowing that the measurements are repeated for 3 consecutive campaigns, the statistics are sufficient to provide a representative image of the average crystal structure of the two oxide layers; including the statistically present tetragonal phase in each case. In other words, it can be claimed that the measurement probes monoclinic zirconia with a given ratio of tetragonal in both cases.
It must be noted that the bulk tetragonal zirconia known in the industry, is always stabilised by large concentrations of different oxides such as yttria, scandia, or ytterbia. Therefore, their composition is not comparable to the phases observed in Zr claddings. The values for the conductivity of bulk monoclinic and tetragonal zirconia are provided in tables 3 and 4 of Appendix A, for comparison.

One other aspect of corrosion can be discussed in the following. Oxidation of Zr based alloys, in

particular in the case of autoclave oxidation, shows a cyclic behaviour [2], [44], meaning that the oxidation process starts at a given rate, it reaches a maximum and then slows down to a minimum rate. In such cases, it has been shown that the correlated hydrogen uptake has a delayed behaviour, either lagging behind and most often increasing in such conditions. This behaviour can be well revealed in autoclave, where the number of samples collected are very large and the oxidation time between two sample can be quite short. In the case of reactor samples, such frequent and condensed sampling methods are not conceivable and samples are scarce. Thus, these corrosion cycles can't be revealed in the same manner. A fuel rod, is extracted from the reactor after a certain number of years (cycles), and the oxidation stage could be anywhere in between two periods. Furthermore, it is possible that such behaviour is even absent in reactor. Therefore, in the case of 9-cycle cladding, the different campaigns performed on different regions of the specimen, could, to some extent reflect these small differences, however, the overall trend, does seem to go in the direction of smaller conducting distance in the 9-cycle oxide compared to the 3-cycle.

The presence of zirconium monoxide has not been detected in the claddings studied here. Therefore, the measurement of a ZrO particle has been carried out only as reference, as reported in the chapter of results. It is also worth noting that the resistivity of this ZrO phase is 5 to 6 orders of magnitude smaller than the oxide at the interface, which means that it is much closer to metal, than to the most conducting oxide measured in the current studies."

Having measured the resistivity profiles of the material after two different residence times, it is necessary to determine the correlation between the variation of resistivity and the variation of hydrogen pickup fraction (HPUF) of the cladding for these two different residence times. The HPUF of these claddings is determined in previous studies and it is observed that the HPUF of 9-cycle cladding is higher than that of 3-cycle cladding (the former is 30% and the latter 17%).

From all our observations and the discussions above, it can be concluded that the material has changed behaviour; leading to different properties, including a change of resistivity. It is demonstrated to a great extent that this change is a consequence of the change of composition (i.e the oxygen concentration of the zirconia as well as the variation of alloying elements present in the oxide at the metal-oxide interface) and the change of micro-porosity. The fact that the resistivity near the interface changes from interface until a distance of 800nm and 1.5 μm (for 9-cycle and 3-cyckle respectively), means that close to the interface, instead of a single layer, an inner, more electronically conductive, layer of oxide is formed. The finding that the resistivity of the 9-cycle cladding for a given distance from the metal-oxide interface is increased corresponds well to the hypothesis that resistivity of the oxide near the interface plays a role on the HPUF and increased resistivity will increase the HPUF.

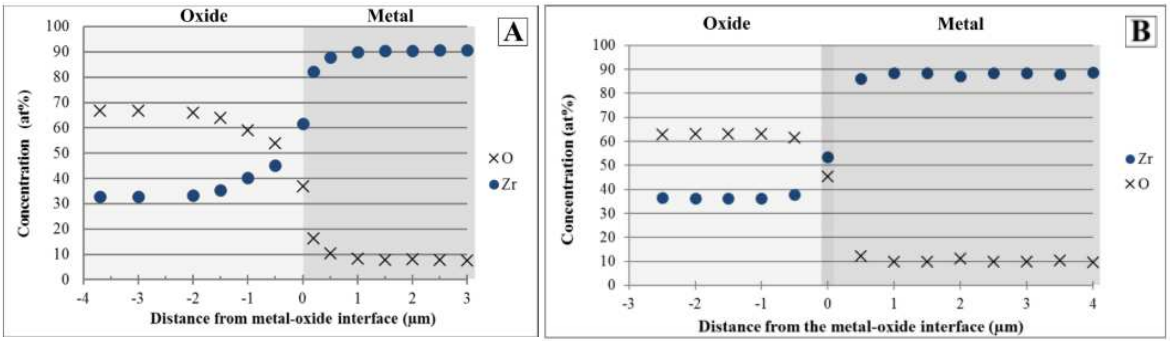

Figure 10. EPMA data of the Oxygen concentration in the vicinity of the metal/oxide interface. a) shows the 3 cycle material and b) shows the 9 cycle. A much longer region of sub-stoichiometry can be seen for the 3-cycle material. These figures have been previously shown in ref [21]

5 Conclusion

This paper presents results of the measurement of the resistivity of the oxide layer formed in the vicinity of the metal-oxide interface of highly irradiated claddings from BWR. The advantage of the method, used to measure the resistivity, is that very site specific properties are probed at high resolutions, by means of micromanipulators and direct measurement in an SEM.
For the first time the resistivity of a Zircaloy-2 cladding, irradiated in a BWR, after two different residence times has been measured and the results have been compared.
The results have shown that:

a- The intrinsic resistivity of oxide in the vicinity of metal-oxide interface varies as a function of distance from the interface.
b- Above a given oxide thickness, this value remains unchanged and no more variation is observed as a function of thickness.
c- The resistivity of 9-cycle cladding at a given distance from the interface is higher than that of 3-cycle cladding.
d- The values of maximum resistivity seem to be similar between the two materials.
e- These findings confirm the hypothesis that the increased hydrogen pickup fraction can be correlated to the increased resistivity of the oxide at a given distance from the interface.
f- The comparison of results with previous studies on the same set of materials, shows that the cause of this increased resistivity is an increased oxygen stoichiometry and in general chemical compositional changes in the oxide, and also owing to an increased micro-crack and micro-pore in the microstructure.

The correlation of the resistivity changes with the chemical composition as well as the other properties such as microcrack pattern and hydrogen uptake provide a valuable information to understand the mechanisms behind the degradation of the material after long-term residence.
Results have clearly shown that the resistivity in the vicinity of metal-oxide interface increases after extreme residence times. However, as these results have demonstrated, above a given oxide thickness (in this case between 2 and 3 μm), the properties of the two oxide films are very similar. It seems that the variations of property for this material are limited to the distances of smaller than 2 micrometres from the metal-oxide interface.

6 Acknowledgements

The authors would like to acknowledge the support of swissnuclear for the PhD project. The supply of the irradiated claddings from KKL is acknowledged to KKL and to Westinghouse Electric Sweden, AB. The team of MUZIC (Mechanistic Understanding of the Zirconium Corrosion) is acknowledged for fruitful discussions.

7 Appendix A

Table 3. Resistance results from three measurement campaigns on three different areas of the sample, for the 3-cycle sample. For each electrode minimum oxide thickness under respective electrodes is shown as well as resistivity values calculated as described in section 2.4.

Measurement number	Minimum thickness (nm)	Resistance (Ohms, Ω)	Resistivity low (Ω.m)	Resistivty high (Ω.m)	Resisitivty average (Ω.m)	Log resistvity average (Ω.m)
Metal-Metal reference						
I	≈100000	3.00E+01	2.43E-07	9.60E-06	4.92E-06	-5.31
II	≈3000000	1.50E+02	4.05E-08	1.60E-06	8.20E-07	-6.09
III	≈200000	5.00E+01	2.03E-07	8.00E-06	4.10E-06	-5.39
Oxide						
I	100	7.00E+04	0.57	22.40	11.48	1.06
II	200	1.00E+04	0.04	1.60	0.82	-0.09
II	240	2.00E+04	0.07	2.67	1.37	0.14
II	290	1.30E+04	0.04	1.43	0.74	-0.13
II	300	1.00E+04	0.03	1.07	0.55	-0.26
II	320	3.00E+05	0.76	30.00	15.38	1.19
II	320	1.00E+05	0.25	10.00	5.13	0.71
III	340	4.00E+05	0.95	37.65	19.30	1.29
II	350	6.50E+05	1.50	59.43	30.47	1.48
II	380	2.00E+05	0.43	16.84	8.63	0.94
II	520	6.00E+05	0.93	36.92	18.93	1.28
II	640	4.00E+06	5.06	200.00	102.53	2.01
III	700	3.60E+06	4.17	164.57	84.37	1.93
III	790	2.00E+05	0.21	8.10	4.15	0.62
I	810	9.50E+06	9.50	375.31	192.40	2.28
III	980	2.20E+07	18.18	718.37	368.28	2.57
II	1030	1.00E+05	0.08	3.11	1.59	0.20
III	1030	4.00E+07	31.46	1242.72	637.09	2.80
III	1030	2.80E+07	22.02	869.90	445.96	2.65
II	1240	4.00E+07	26.13	1032.26	529.19	2.72
I	1320	7.50E+07	46.02	1818.18	932.10	2.97
III	1330	1.00E+08	60.90	2406.02	1233.46	3.09
II	1670	6.00E+08	291.02	11497.01	5894.01	3.77
I	1870	7.00E+08	303.21	11978.61	6140.91	3.79
III	1900	2.20E+07	9.38	370.53	189.95	2.28
III	2100	2.20E+07	8.49	335.24	171.86	2.24
III	2300	3.50E+08	123.26	4869.57	2496.41	3.40
II	2990	1.00E+09	270.90	10702.34	5486.62	3.74

II	3260	1.00E+09	248.47	9815.95	5032.21	3.70

Table 4. Resistance results for the 9-cycle sample from three measurement campaigns on three different areas of the sample. For each electrode minimum oxide thickness under respective electrodes is shown as well as resistivity values calculated as described in section 2.4.

Measurement number	Minimum thickness (nm)	Resistance (Ohms, Ω)	Resistivity low (Ω.m)	Resistivty high (Ω.m)	Resisitivty average (Ω.m)	log resistvity average (Ω.m)
Metal-Metal reference						
I	100000	3.00E+01	2.43E-07	9.60E-06	4.92E-06	-5.31
II	150000	3.00E+01	1.62E-07	6.40E-06	3.28E-06	-5.48
III	200000	5.00E+01	2.03E-07	8.00E-06	4.10E-06	-5.39
Oxide						
I	300	5.00E+04	0.14	5.33	2.73	0.44
II	450	7.00E+06	12.60	497.78	255.19	2.41
II	480	7.00E+06	11.81	466.67	239.24	2.38
III	590	2.10E+07	28.83	1138.98	583.91	2.77
III	670	2.60E+07	31.43	1241.79	636.61	2.80
II	770	5.50E+07	57.86	2285.71	1171.79	3.07
I	850	2.00E+08	190.59	7529.41	3860.00	3.59
III	1200	4.30E+08	290.25	11466.67	5878.46	3.77
III	1320	4.40E+08	270.00	10666.67	5468.33	3.74
III	1450	5.70E+08	318.41	12579.31	6448.86	3.81
I	1480	4.30E+08	235.34	9297.30	4766.32	3.68
II	1740	7.00E+08	325.86	12873.56	6599.71	3.82
II	2000	6.50E+08	263.25	10400.00	5331.63	3.73
II	2300	7.00E+08	246.52	9739.13	4992.83	3.70
I	2440	5.00E+08	165.98	6557.38	3361.68	3.53
I	2950	1.50E+09	411.86	16271.19	8341.53	3.92
I	3760	2.50E+09	538.56	21276.60	10907.58	4.04
I	4300	1.00E+09	188.37	7441.86	3815.12	3.58
I	4800	2.80E+09	472.50	18666.67	9569.58	3.98

8 References

[1] D. O. Northwood, "The Development and Applications of Zirconium Alloys," *Mater. Des.*, vol. 6, no. 2, pp. 143–149, 1985.

[2] A. T. Motta, A. Couet, and R. J. Comstock, "Corrosion of Zirconium Alloys Used for Nuclear Fuel Cladding," *Annu. Rev. Mater. Res.*, vol. 45, no. 1, pp. 311–343, 2015.

[3] A. T. Motta and L. Q. Chen, "Hydride formation in zirconium alloys," *Jom*, vol. 64, no. 12, pp. 1403–1408, 2012.

[4] B. Cox, K. VG, and L. C, "Waterside corrosion of zirconium alloys in nuclear power plants," *IAEA Tecdoc*, no. January, pp. 1–313, 1998.

[5] S. Kass, "Hydrogen Pickup in Various Zirconium Alloys during Corrosion Exposure in High-Temperature Water and Steam," *J. Electrochem. Soc.*, vol. 107, no. 7, pp. 594–597, 1960.

[6] S. Abolhassani *et al.*, "Corrosion and hydrogen uptake in zirconium claddings irradiated in light water reactors," *Zircon. Nucl. Ind. 17th Int. Symp. ASTM STP 1543*, vol. 1543, pp. 540–573, 2015.

[7] A. Couet, A. T. Motta, and R. J. Comstock, "Effect of Alloying Elements on Hydrogen Pickup in Zirconium Alloys," *Zircon. Nucl. Ind. 17th Vol.*, pp. 479–514, 2015.

[8] A. Couet, A. T. Motta, A. Ambard, and D. Livigni, "In-situ electrochemical impedance spectroscopy measurements of zirconium alloy oxide conductivity: Relationship to hydrogen pickup," *Corros. Sci.*, vol. 119, pp. 1–13, 2017.

[9] M. Lindgren and I. Panas, "Oxygen Vacancy Formation, Mobility, and Hydrogen Pick-up during Oxidation of Zirconium by Water," *Oxid. Met.*, vol. 87, no. 3–4, pp. 355–365, 2017.

[10] J. Schefold, D. Lincot, A. Ambard, and O. Kerrec, "The Cyclic Nature of Corrosion of Zr and Zr-Sn in High-Temperature Water „ 633 K … A Long-Term In Situ Impedance Spectroscopic Study," pp. 451–461, 2003.

[11] V. Renčiuková, J. Macák, P. Sajdl, R. Novotný, and A. Krausová, "Corrosion of zirconium alloys demonstrated by using impedance spectroscopy," *J. Nucl. Mater.*, vol. 510, pp. 312–321, 2018.

[12] J. J. Vermoyal, A. Frichet, L. Dessemond, and A. Hammou, "AC impedance study of corrosion films formed on zirconium based alloys," *Electrochim. Acta*, vol. 45, no. 7, pp. 1039–1048, 1999.

[13] R. K. Münch, G. Bart, O. Gebhardt, and D. Landolt, "Investigation of Zircaloy-4 Oxidation under Simulated Pressurised Water Reactor Conditions Using Electrochemical Impedance Spectroscopy," *Mater. Sci. Forum*, vol. 289–292, pp. 163–168, 1998.

[14] P. Barberis and A. Frichet, "Characterization of Zircaloy-4 oxide layers by impedance spectroscopy," vol. 273, pp. 182–191, 1999.

[15] J. K. Stortelder, "Ionic Conductivity in Yttria-Stabilized Zirconia Thin Films grown by Pulsed Laser Deposition," *Inorg. Mater. Sci.*, no. August, 2005.

[16] X. Guo, "Hydrothermal degradation mechanism of tetragonal zirconia," *J. Mater. Sci.*, vol. 36, no. 15, pp. 3737–3744, 2001.

[17] R. Vanta and S. Abolhassani, "Study of the change of semiconducting properties of the oxide at the vicinity of metal-oxide interfaces in fuel rods," *Master Thesis EPFL*, 2015.

[18] R. Vanta, S. Abolhassani, and M. Dadras, "Examination of semiconducting properties of oxides in the vicinity of metal-oxide interfaces for selected alloys," *Eur. Microsc. Congr. 2016 Proc.*, vol. 399, no. 1, pp. 382–383, 2016.

[19] A. Baris *et al.*, "Chemical and microstructural characterization of a 9 cycle Zircaloy-2 cladding using EPMA and FIB tomography," *J. Nucl. Mater.*, vol. 504, pp. 144–160, 2018.

[20] S. Abolhassani, R. Restani, and L. Hallstadius, "Comparative analysis of the evolution of Zircaloy-2 cladding irradiated in BWR," *Top Fuel React. Perform. 2015. Conf. Proc. Poster*, pp. 272–298, 2015.

[21] A. Baris, "INCREASED HYDROGEN UPTAKE OF ZIRCONIUM BASED CLADDINGS AT HIGH BURNUP," *A thesis Submitt. to Univ. Birmingham degree Dr. Philos. Sch. Metall. Mater. Univ. Birmingham*, no. March, 2019.

[22] A. Baris, S. Abolhassani, Y. L. Chiu, and H. E. Evans, "Observation of crack microstructure in oxides and its correlation to oxidation and hydrogen-uptake by 3D FIB Tomography – case of

Zr-ZrO $_2$ in reactor," *Mater. High Temp.*, vol. 3409, pp. 1–8, 2017.
[23] A. W. Colldeweih, A. Baris, P. Spätig, and S. Abolhassani, "Evaluation of mechanical properties of irradiated zirconium alloys in the vicinity of the metal-oxide interface," *Mater. Sci. Eng. A*, vol. 742, no. April 2018, pp. 842–850, 2019.
[24] M. M. R. Howlader, K. Shiiyama, C. Kinoshita, M. Kutsuwada, and M. Inagaki, "The electrical conductivity of zircaloy oxide films," *J. Nucl. Mater.*, vol. 253, no. 1–3, pp. 149–155, 1998.
[25] S. Abolhassani *et al.*, "TEM Examinations of the Metal-Oxide Interface of Zirconium Based Alloys Irradiated in a Pressurized Water Reactor," *J. ASTM Int.*, vol. 2, no. 6, p. 12390, 2005.
[26] A. T. Motta *et al.*, "Microstructure and growth mechanism of oxide layers formed on Zr alloys studied with micro-beam synchrotron radiation," *Zircon. Nucl. Ind. 14th Int. Symp.*, vol. 1467, no. 5, pp. 205–232, 2005.
[27] B. Cox, "Some thoughts on the mechanisms of in-reactor corrosion of zirconium alloys," *J. Nucl. Mater.*, vol. 336, no. 2–3, pp. 331–368, 2005.
[28] R. M. Pashley, M. Rzechowicz, L. R. Pashley, and M. J. Francis, "De-gassed water is a better cleaning agent," *J. Phys. Chem. B*, vol. 109, no. 3, pp. 1231–1238, 2005.
[29] B. Cox, J. P. Pemsler, and D. Bchantillons, "Diffusion of oxygen in growing zirconia films," *J. Nucl. Mater.*, vol. 28, pp. 73–78, 1968.
[30] S. Abolhassani, G. Bart, and A. Jakob, "Examination of the chemical composition of irradiated zirconium based fuel claddings at the metal/oxide interface by TEM," *J. Nucl. Mater.*, vol. 399, no. 1, pp. 1–12, 2010.
[31] A. Atkinson, "Wagner theory and short circuit diffusion," *Mater. Sci. Technol.*, vol. 4, no. 12, pp. 1046–1051, 1988.
[32] A. T. Fromhold, "Theory of Metal Oxidation," *North Holl. Publ. Co.*, pp. 1–16, 1976.
[33] N. M. TALLAN and R. W. VEST, "Electrical Properties and Defect Structure of Y2O3," *J. Am. Ceram. Soc.*, vol. 49, no. 8, pp. 401–404, 1966.
[34] R. Collongues, "La non-stœchiométrie," *Masson cie, Ed. Paris*, pp. 40-64., 1971.
[35] A. Sinhamahapatra, J. P. Jeon, J. Kang, B. Han, and J. S. Yu, "Oxygen-Deficient Zirconia (ZrO2-x): A New Material for Solar Light Absorption," *Sci. Rep.*, vol. 6, no. May, pp. 1–8, 2016.
[36] J. Shin, J. H. Joo, D. Samuelis, and J. Maier, "Oxygen-Deficient TiO2−δ Nanoparticles via Hydrogen Reduction for High Rate Capability Lithium Batteries," *Chem. Mater.*, vol. 24, no. 3, pp. 543–551, 2012.
[37] A. M. A. A. H. Al-mowali, "Doping , Vacancy formation and Substitutional Effects on Semiconductor Selectivity of Rutile TiO 2 Crystal," vol. 3, no. 2, pp. 22–32, 2013.
[38] B. J. Morgan and G. W. Watson, "Erratum: Intrinsic n-type defect formation in TiO 2: A comparison of rutile and anatase from GGA+ U calculations (Journal of Physical Chemistry C (2010) 114:5 (2321-2328) DOI: 10.1021/jp9088047)," *J. Phys. Chem. C*, vol. 116, no. 12, p. 7242, 2012.
[39] L. Liu *et al.*, "Oxygen vacancies: The origin of n-type conductivity in ZnO," *Phys. Rev. B*, vol. 93, no. 23, 2016.
[40] G. Ledergerber *et al.*, "Fuel performance beyond design - Exploring the limits," *LWR Fuel Perform. Meet. Fuel/WRFPM 2010*, pp. 513–524, 2010.
[41] A. Couet, A. T. Motta, and A. Ambard, "The coupled current charge compensation model for zirconium alloy fuel cladding oxidation: I. Parabolic oxidation of zirconium alloys," *Corros. Sci.*, vol. 100, pp. 73–84, 2015.
[42] D. S. Rutmal et al, "Relationship between electric resistance of zirconia ceramics and porosity," *UDC 666.764.262.315.592*, no. 6, pp. 36–39, 1970.
[43] M. Chollet *et al.*, "Synchrotron X-ray diffraction investigations on strains in the oxide layer of an irradiated Zircaloy fuel cladding," *J. Nucl. Mater.*, vol. 488, pp. 181–190, 2017.
[44] J. Romero, J. Partezana, R. J. Comstock, L. Hallstadius, A. T. Motta, and A. Couet, "Evolution of Hydrogen Pickup Fraction with Oxidation Rate on Zirconium Alloys," *Top Fuel React. Fuel Perform.*, pp. 1–7, 2015.

Declaration of interests

☒ The authors declare that they have no known competing financial interests or personal relationships that could have appeared to influence the work reported in this paper.

☒The authors declare the following financial interests/personal relationships which may be considered as potential competing interests:

Jonathan Hawes on behalf of all authors